

Overriding plate thickness as a controlling factor for trench retreat rates in narrow subduction zones

Pedro J. Gea^{1,2}, Flor de Lis Mancilla^{1,2}, Ana M. Negredo^{3,4}, and Jeroen van Hunen⁵

¹Department of Theoretical Physics and Cosmology, University of Granada, Granada, Spain

²Andalusian Institute of Geophysics, University of Granada, Granada, Spain

³Department of Earth Physics and Astrophysics, Complutense University of Madrid, Madrid, Spain

⁴Institute of Geosciences IGEO (CSIC, UCM), Madrid, Spain

⁵Department of Earth Sciences, Durham University, DH1 3LE Durham, UK

Key Points:

- Three-dimensional numerical models of narrow subduction zones including all plates are performed to study trench kinematics
- Overriding plate thickness is the main factor affecting trench retreat velocities in narrow subduction zones
- The overriding plate has an important role in modulating trench geometries

Abstract

Slab width plays a major role in controlling subduction dynamics and trench motion. However, observations on natural narrow subduction zones do not show any correlation between slab width and trench velocities, indicating that other factors may have a greater impact. Here, we use 3D numerical subduction models to evaluate the effect of slab width, strength of slab coupling to the lateral plate and overriding plate thickness on trench kinematics. Model results show that slab width has little influence on trench migration rates for narrow subduction zones, but that the thickness of the overriding plate plays a major role, with trench velocities decreasing as the thickness increases. These results explain trench velocities observed in natural narrow subduction zones showing no relation with slab width but an inverse dependence on overriding plate thickness. Finally, we find that the overriding plate thickness also significantly affects the trench shape.

Plain Language Summary

Subduction zones are the main drivers of plate tectonics and control much of the seismic and volcanic activity on Earth. For that reason, subduction processes have been widely studied in the last few decades. Because of the limited amount of available data, one of the key techniques has been numerical modelling. Some earlier models have shown that the velocity of the trench (long region marking where subduction starts) is affected by the width of the subduction zone, but this is not observed for narrow subduction zones in nature. In this work, we model 3D narrow subduction systems and find that the thickness of the unsubducted overriding plate affects trench velocities much more than the width of the subduction zone: the thicker the plate, the slower the trench motion. Moreover, the thickness of the overriding plate affects the shape that the trench develops. Our models explain some key observations in Earth's narrow subduction zones and help to better understand these processes.

1 Introduction

Subducting slabs are the main drivers of plate motion and flow in Earth's mantle. Thus, much effort has been put in the last few decades into understanding the main factors controlling slab dynamics and subduction-induced mantle flow (e.g., Billen, 2008; Funiciello et al., 2003; Gerya, 2022; Schellart, 2004; Stegman et al., 2010; van Hunen & Allen, 2011). Previous geodynamic modelling studies have shown the wide variety of physical parameters that influence subduction processes, such as the slab thickness (Bellahsen et al., 2005; Capitanio & Morra, 2012; F. Chen et al., 2022; Funiciello et al., 2008; Stegman et al., 2010) and length (A. F. Holt & Becker, 2016; Xue et al., 2020), the mantle rheology (A. F. Holt & Becker, 2016; Pusok et al., 2018), the strength and thickness of the overriding plate (OP) (Butterworth et al., 2012; Hertgen et al., 2020; A. Holt et al., 2015; Meyer & Schellart, 2013; Rodríguez-González et al., 2014; Sharples et al., 2014), the slab-mantle viscosity contrast (Funiciello et al., 2008; Schellart, 2008; Stegman et al., 2010), the coupling at the subduction-interface (Čížková & Bina, 2013, 2019; Behr et al., 2022) or the mechanical boundary conditions (Z. Chen et al., 2015; Funiciello et al., 2004). All these studies highlight the complexity of subduction, which makes these processes still incompletely understood in their key aspects (Gerya, 2022).

Among the factors controlling subduction dynamics, the slab width (W) has been shown to be of major importance (Bellahsen et al., 2005; F. Chen et al., 2022; Di Giuseppe et al., 2008; Guillaume et al., 2010, 2021; Royden & Husson, 2006; Schellart et al., 2007; Stegman et al., 2006, 2010; Strak & Schellart, 2016). Earlier geodynamic studies have distinguished three types of trench curvature depending on slab width: concave for narrow slabs ($W \leq 1500$ km), "w"-shaped (also referred to as sublinear) for intermediate width slabs ($W \sim 2000\text{--}3000$ km) and convex for wide slabs ($W \geq 4000$ km) (Schellart et al., 2007; Stegman et al., 2010; Strak & Schellart, 2016), although the exact values differentiating these regimes

66 depend somewhat on the specific conditions. In addition, the slab dip seems to be controlled
 67 by W, increasing (producing steeper slabs) with wider subducting plates (Schellart, 2004;
 68 Strak & Schellart, 2016). W also controls the subduction-induced mantle flow (Piromallo et
 69 al., 2006; Stegman et al., 2006), causing faster and more localized mantle upwellings near the
 70 lateral slab edges for wider slabs (Strak & Schellart, 2016). Regarding the slab kinematics,
 71 previous studies have shown that the trench retreat velocity (V_T) decreases as the slab
 72 becomes wider (F. Chen et al., 2022; Schellart, 2004; Schellart et al., 2007; Stegman et al.,
 73 2006). All these studies provide useful insights that help to understand the effect of W on
 74 subduction processes. However, most of these model setups that specifically focused on slab
 75 width had no OP, which is known to affect subduction dynamics significantly (e.g., Hertgen
 76 et al., 2020; Magni et al., 2014; Yamato et al., 2009). Additionally, the inverse dependence
 77 of V_T on W predicted by some models is not observed in natural narrow subduction zones
 78 (e.g., Calabria, Gibraltar, Scotia), which do not show any correlation between W and V_T ,
 79 suggesting that other factors may play a more relevant role on trench retreat velocities.
 80 Incorporating an OP can help to better understand the effect of W on V_T and the dominant
 81 factors controlling trench retreat rates in narrow subduction zones.

82 In this study, we have conducted self-consistent 3D numerical subduction models to
 83 systematically evaluate in narrow subduction zones the effect of slab width, overriding plate
 84 thickness and coupling of the slab with the lateral plate on trench motion. In order to
 85 model realistic subduction processes, we have included the subducting and surrounding
 86 plates (lateral and overriding). Based on our geodynamic models and a comparison with
 87 observations in nature, this work explores the factors dominating trench retreat velocities in
 88 narrow subduction zones and provides new insights on the role of the OP in trench motion.

89 2 Methods

90 The simulations have been performed with version 2.4.0 of the finite-element code
 91 ASPECT (Advanced Solver for Problems in Earth's ConvecTion) (Kronbichler et al., 2012;
 92 Heister et al., 2017; Gassmöller et al., 2018; Bangerth et al., 2021a, 2021b). We have
 93 used the Boussinesq approximation to solve the coupled conservation equations for mass,
 94 momentum and energy, which assumes that the density is constant in all equations except
 95 in the buoyancy term of the momentum equation (Text S1 in the supporting information).

96 The initial 3-D model setup is shown in Figure 1. The initial geometry has been built
 97 using the Geodynamic World Builder (GWB) version 0.4.0 (Fraters et al., 2019, 2021) and
 98 it measures 2000x800x660 km in the x, y and z directions. Because the XZ plane at y = 0 is
 99 a plane of symmetry (Figure 1), we only model one half of the subduction zone. The initial
 100 geometry consists of an ongoing subduction system with a 220 km-long slab and a dip angle
 101 of 40°. In this way, the model is self-driven by buoyancy and the rest of internal forces.
 102 The subducting plate (SP) is comprised of weak crust 10 km thick and lithospheric mantle
 103 85 km thick. The weak crust allows for the decoupling of the slab from the top surface and
 104 from the OP to facilitate subduction. The SP width is varied between models in the range
 105 of 400-1200 km. The OP has an initial thickness of 70 km, consisting of a 30 km crust
 106 and a 40 km lithospheric mantle, although its thickness also varies between models. The
 107 lateral plate (LP) is completely made of lithosphere 95 km thick, without any compositional
 108 stratification. We use a zone 20 km wide (transform fault) as a mechanical coupling of the
 109 lateral plate with the other plates. The trench is initially located at x = 1000 km, and we
 110 use particles placed along its length to track its movement over the time. The inclusion of
 111 the OP and LP provides a reasonable model setup and avoids unrealistic behaviour since
 112 the presence of these plates strongly affects the subduction dynamics (e.g., Yamato et al.,
 113 2009). For example, previous studies have shown that the presence of an OP results in a
 114 slowdown of the trench retreat velocities, highlighting that the poloidal flow is affected by
 115 the coupling of the subducting and overriding plate (e.g., Capitanio et al., 2010; Yamato et
 116 al., 2009). Regarding the role of the LP, its inclusion in subduction models prevents lateral
 117 shortening (Yamato et al., 2009).

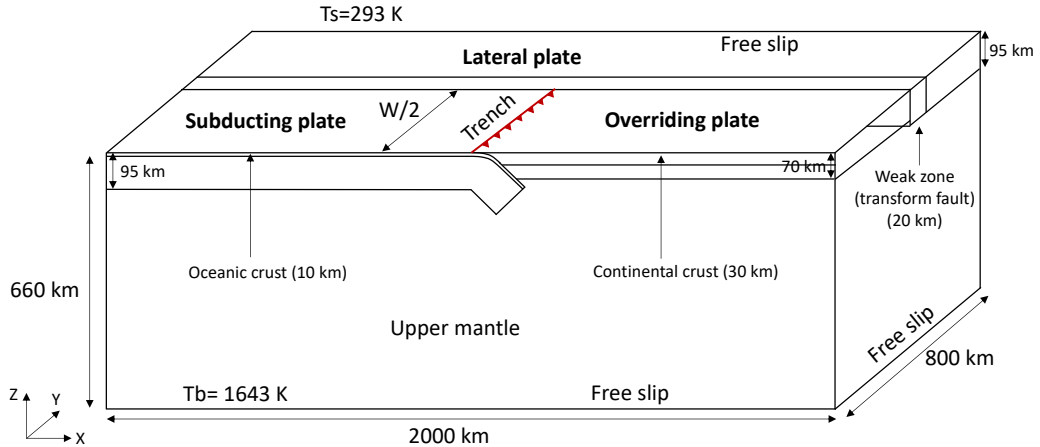


Figure 1. Three-dimensional model setup and boundary conditions. The setup includes a subducting plate (SP), an overriding plate (OP) and a lateral plate (LP). W indicates slab width and the red line with triangles marks the initial trench position at $x = 1000$ km. The trench is plotted for the whole subduction zone in Figures 2 and 3. The temperature is fixed to 293 K at the top boundary and 1643 K at the bottom boundary. All boundaries are free slip. Note that only half of the subduction zone is modelled due to the symmetry of the problem.

The initial temperature profile increases linearly from 293 K at the surface to 1643 K at the lithosphere-asthenosphere boundary (LAB). For the top and bottom boundaries we use Dirichlet temperature conditions. All boundaries are free slip, which means that the velocity perpendicular to the boundaries is prescribed to 0 (Dirichlet boundary condition) and that there are no stresses parallel to the boundary (Neumann boundary condition). In terms of rheology, we use a temperature-dependent viscosity (Text S2 and Table S1 in the supporting information) except for the subducting plate crust and weak zone where we impose constant viscosities of 10^{20} Pa s. With this rheology, we obtain a viscosity of $1.57 \cdot 10^{20}$ Pa s at a depth of 150 km. Finally, we impose cutoffs of $1 \cdot 10^{19}$ and $1.57 \cdot 10^{23}$ Pa s (1000 times the upper mantle viscosity at a depth of 150 km) to avoid large viscosity jumps. All model parameters are listed in Table S1 in the supporting information.

3 Results

3.1 Effect of slab width and coupling at the lateral slab edge

In order to study narrow subduction zones, we performed experiments varying W in the range of 400 to 1200 km. For each experiment, we have tested different amounts of mechanical coupling of the slab with the lateral plate by changing the viscosity of the transform fault (μ_{TF}) (experiments 1-15, Table S2 in the supporting information).

The subduction dynamics is similar in all the experiments. Initially, the slab freely sinks into the upper mantle due to the density contrast and the trench retreat velocities quickly increase (Figure 2d), accompanied by slab rollback and inducing toroidal flow around the slab edges (Figure S1 in the supporting information). All models show the maximum V_T when the slab tip reaches ~ 400 km depth. Thereafter, trench velocities slightly decrease due to the interaction of the slab tip with the deep viscous upper mantle, and approach a roughly constant value (Figure 2d).

Figures 2a-2d show the trench kinematics for a weak slab coupling to the lateral plate ($\mu_{TF} = 10^{20}$ Pa s). Models develop two types of trench geometries in the center of the

144 subduction zone depending on W. The trench in models with $W \leq 1000$ km shows a concave
 145 geometry toward the overriding plate, with the trench in the center of the subduction zone
 146 retreating faster than its edges (Figures 2a and 2b). This characteristic geometry is attained
 147 earlier in models with smaller W. For example, the concave geometry for $W = 400$ km is
 148 almost achieved in 2 Myr, while for $W = 600$ km it is not attained until 10 Myr. For the
 149 model with $W = 1200$ km, the trench geometry is rectilinear in its center up to 10 Myr, and
 150 thereafter adopts a “w”-shape, with retreat velocities being higher in between the lateral
 151 slab edge and the center of the subduction zone (Figure 2c). The highest V_T is found for
 152 $W = 600$ km and decreases for wider slabs (Figure 2d and blue line in Figure 2e).

153 Concerning the mechanical coupling of the slab with the lateral plate, we find that
 154 the maximum V_T correlates positively with W for $W \leq 600$ km when the viscosity of the
 155 transform fault is $\mu_{TF} = 10^{20}$ Pas, but for $W \leq 800$ km when $\mu_{TF} = 10^{21}$ or $\mu_{TF} = 10^{22}$
 156 Pas (Figure 2e). The maximum V_T decreases as the viscous coupling increases for $W \leq$
 157 800 km, but does not change significantly for $W > 800$ km. The fact that the three curves
 158 in Figure 2e tend to converge with W approaching 1200 km indicates that effect of the
 159 strength of lateral coupling on V_T is only significant for very narrow subduction zones, and
 160 give maximum V_T differences about 1.8 cm/yr for $W = 400$ km. Finally, increasing the
 161 viscous coupling to the lateral plate also results in more concave trench geometries. For a
 162 W of 1200 km, we obtain “w”-shapes for $\mu_{TF} = 10^{20}$ and $\mu_{TF} = 10^{21}$ Pas and concave
 163 geometries for $\mu_{TF} = 10^{22}$ Pas (Figure S2 in the supporting information).

164 3.2 Effect of overriding plate thickness

165 We have varied the overriding plate thickness in the range of 40 to 100 km to study its
 166 effect on trench motion (experiments 2 and 16-21, Table S2 in the supporting information).
 167 In our models, the trench develops a concave geometry in all cases (Figures 3a, 3c and 3d)
 168 except for an OP thickness of 100 km, where a “w”-shape develops after about 10 Myr
 169 of evolution (Figure 3b), showing that thick overriding plates facilitates the formation of
 170 such geometries. Significant trench lateral shortening is also observed as the OP thickness
 171 increases (Figures 3b and 3d). Regarding the kinematics, V_T significantly decreases with
 172 thicker overriding plates (Figure 3e). For example, the maximum V_T is ~ 6.8 cm/yr with
 173 an OP 40 km thick and decreases to ~ 5.4 cm/yr with an OP 60 km thick. Short periods
 174 of small trench advance at the beginning of the simulation occur for OP thicknesses greater
 175 than 70 km (Figure 3e).

176 4 Discussion

177 4.1 Comparison with previous studies

178 Our geodynamic models provide new insights into the effect of W, OP thickness and
 179 strength of slab coupling to the lateral plate on trench kinematics. We find two out of the
 180 three types of trench geometries identified by Schellart et al. (2007), Stegman et al. (2010)
 181 and Strak and Schellart (2016) but for a different range of W values. The numerical models
 182 of Schellart et al. (2007) and Stegman et al. (2010) suggest values of $W \leq 1500$ km, W
 183 $\sim 2000\text{-}3000$ km and $W \geq 4000$ km leading to concave, “w”-shaped and convex trenches,
 184 while the analog models of Strak and Schellart (2016) indicate values of $W = 2000\text{-}2500$
 185 km and $W \geq 3000$ km for “w”-shaped and convex geometries respectively. The analog
 186 modelling of Guillaume et al. (2021) predicts concave and “w”-shaped geometries even for
 187 wider slabs ($W = 2000$ and $W = 4000$ km respectively). Similarly, the recent 3-D spherical
 188 shell numerical models of F. Chen et al. (2022) place the transition from concave trenches to
 189 “w”-shaped geometries at a W of 2400 km for their reference case. Our results do not show
 190 convex geometries, which is expected as we focus only on narrow subduction zones and these
 191 geometries are found for very wide slabs (Schellart et al., 2007; Strak & Schellart, 2016).
 192 However, our models show a “w”-shaped geometry for a much narrower slab ($W = 1200$
 193 km, Figure 2c) than in previous studies ($W \geq 2000$). Following our results, a likely factor

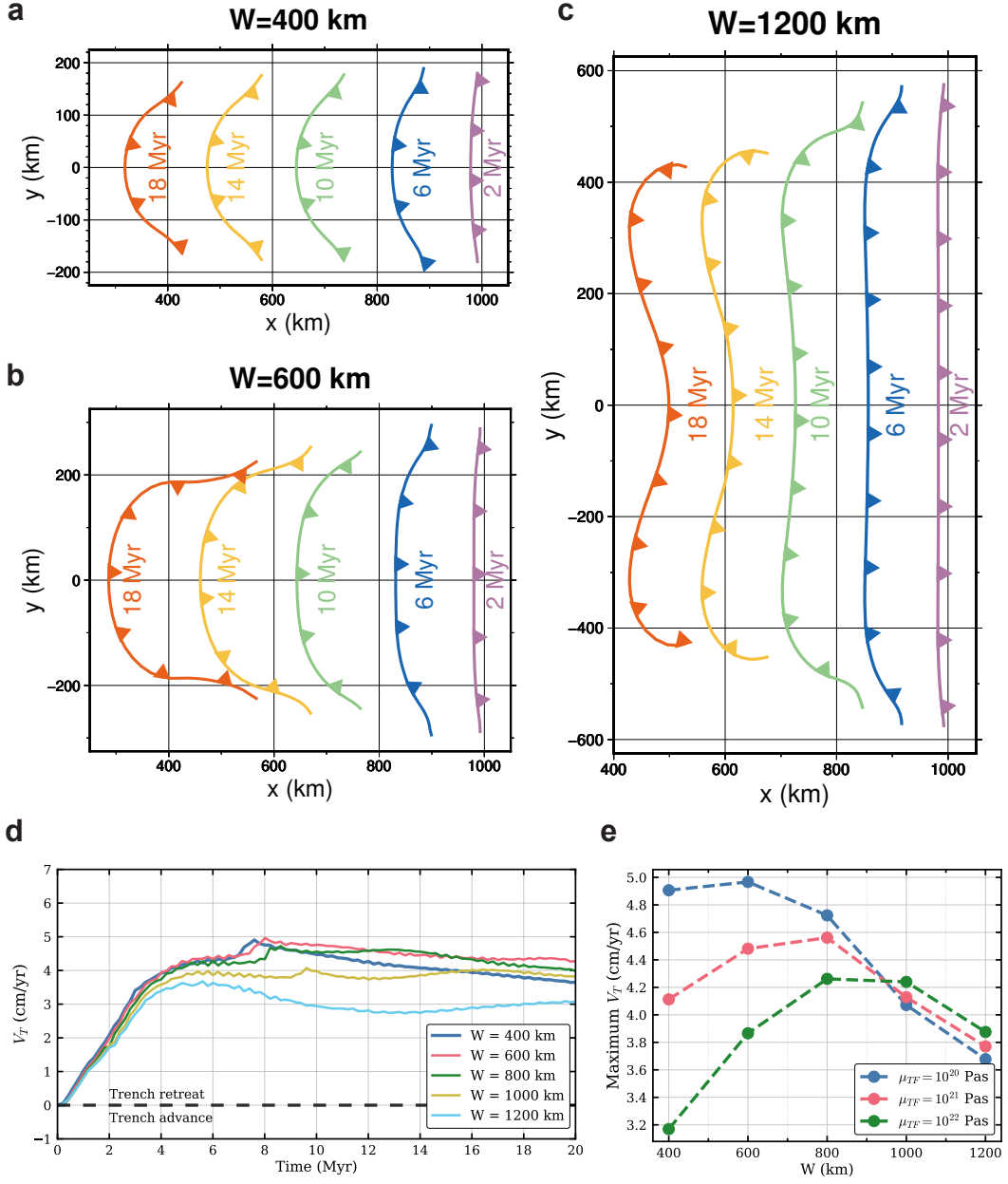


Figure 2. (a-c) Evolution of the subduction trench for three simulations with (a) $W = 400 \text{ km}$, (b) $W = 600 \text{ km}$ and (c) $W = 1200 \text{ km}$. Note that the entire trench is plotted but we only model half of the subduction zone. (d) V_T over time (measured in the center of the subduction zone) for simulations with different W . Panels (a-d) show the results for a $\mu_{TF} = 10^{20} \text{ Pas}$. (e) Maximum V_T at the center of the subduction zone for different W and different viscous coupling at the lateral slab edge.

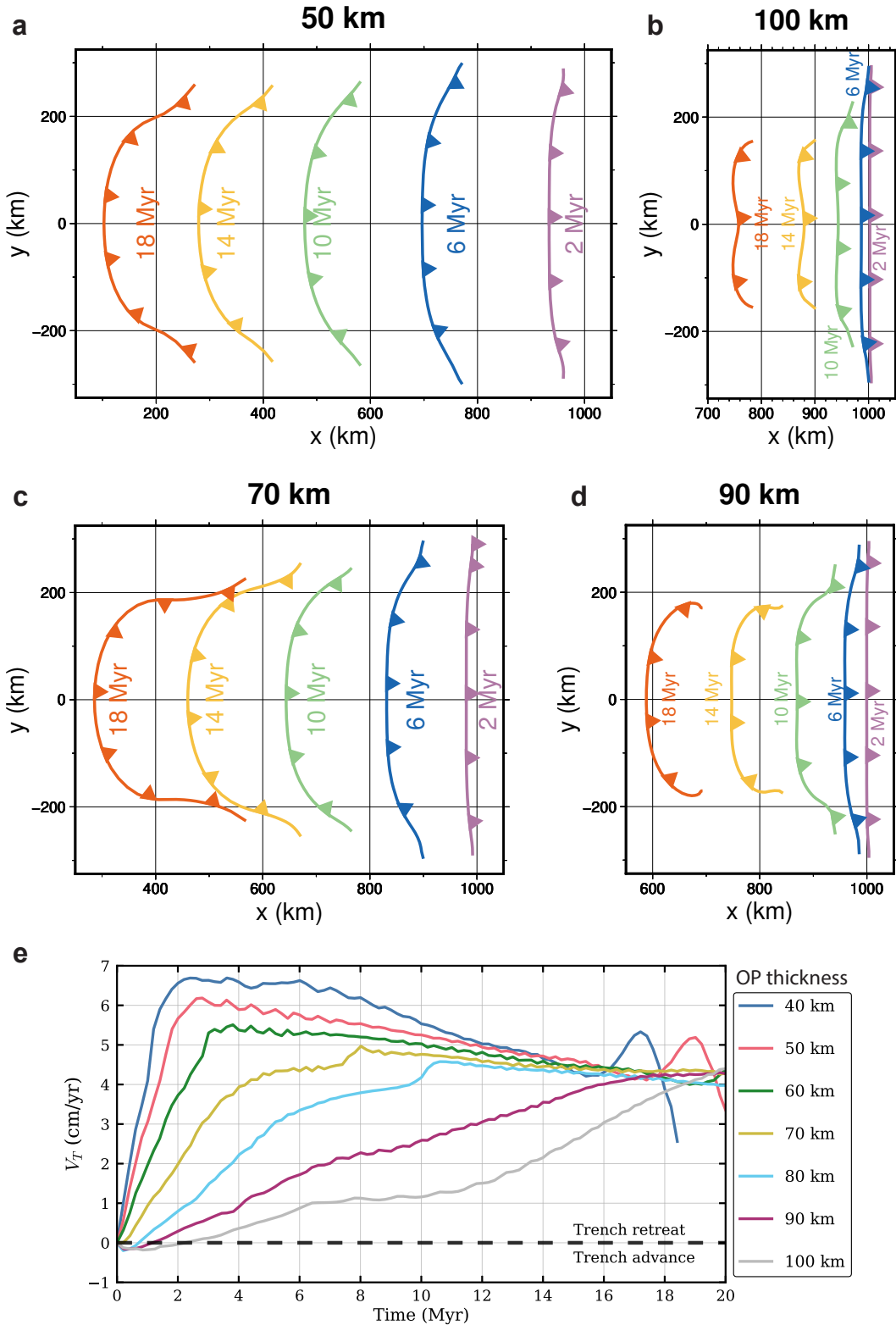


Figure 3. (a-d) Evolution of the subduction trench for four simulations with OP thicknesses of (a) 50 km, (b) 100 km, (c) 70 km and (d) 90 km. Note that the entire trench is plotted but we only model half of the subduction zone. (e) V_T over time (measured in the center of the subduction zone) for simulations with different OP thicknesses.

194 that could explain these discrepancies is the influence of the OP, which was not included in
 195 such previous studies. In fact, our results show that increasing the OP thickness in models
 196 with the same W leads to “w”-shaped trenches (Figure 3b).

197 Regarding trench migration velocities, previous modelling studies have found that V_T
 198 decreases with increasing W (e.g., F. Chen et al., 2022; Schellart et al., 2007; Stegman et
 199 al., 2006). However, this behaviour is not always maintained for narrow subduction zones.
 200 Our results show a direct dependence of V_T on W for $W \leq 600$ km when the mechanical
 201 coupling of the slab with the lateral plate is weak ($\mu_{TF} = 10^{20}$ Pa s) and for $W \leq 800$ km
 202 when the coupling is stronger ($\mu_{TF} = 10^{21}$ and $\mu_{TF} = 10^{22}$ Pa s) (Figure 2e). This positive
 203 correlation between V_T and W has also been suggested in previous works for $W \leq 500$ -
 204 600 km (Schellart, 2004; Stegman et al., 2006) and for $W \leq \sim 1000$ km (Strak & Schellart,
 205 2016). Our models using a weak coupling are in agreement with the results of Stegman et
 206 al. (2006) finding a maximum retreat velocity for $W = 600$ km. The difference between the
 207 present work and previous studies on which slab width exhibits the highest V_T suggests a
 208 dependence on different model parameters and setup. For example, our models show that
 209 the W for which V_T peaks increases as the viscous coupling at the transform fault becomes
 210 stronger (Figure 2e). More research is needed to clarify the dynamics and factors affecting
 211 this phenomenon. Here we propose that a peak V_T is observed in Figure 2e due to an
 212 energy balance (Magni et al., 2014) between the available gravitational potential energy of
 213 the slab E_{pot} and the energy required for frictional dissipation in the mantle $E_{diss,m}$ and at
 214 the transform fault $E_{diss,TF}$. For relatively wide slabs, $E_{diss,TF}$ is relatively unimportant,
 215 E_{pot} linearly increases with slab width, while $E_{diss,m}$ increases faster than that. So trench
 216 retreat is slower for wider slabs. For narrow slabs, E_{pot} and $E_{diss,m}$ are both small, and
 217 $E_{diss,TF}$ becomes more important. Since E_{pot} decreases for narrowing slabs, while $E_{diss,TF}$
 218 is independent of slab width, narrow slabs retreat slower than wider slabs. Finally, our
 219 models demonstrate the strong impact of the OP thickness on trench retreat velocities,
 220 with V_T decreasing significantly with increasing OP thickness (Figure 3e). This result is in
 221 agreement with the recent 3D numerical modelling including a SP and OP by Hertgen et al.
 222 (2020), who found that thin/weak OP favours faster trench velocities and rollback compared
 223 to a thick/strong OP. The 2D self-consistent subduction models of Gea et al. (2023) and
 224 A. Holt et al. (2015) also show that a thicker OP leads to a reduction in V_T . Increasing the
 225 thickness of the OP limits the space for the induced mantle to flow beneath it, thus reducing
 226 the interaction between the slab and the poloidal flow and resulting in lower trench retreat.

227 4.2 Comparison with nature

228 Natural subduction zones on Earth are influenced by a large number of factors that
 229 are not included in our models, such as slabs of non-uniform age, complex slab morpholo-
 230 gies or plate velocities. Thus, comparing our results with observations on Earth should
 231 be approached with caution, being aware of the inherent limitations. Nevertheless, our
 232 geodynamic model predictions are useful to explain some observations on natural narrow
 233 subduction zones.

234 The concave trench geometries predicted by our geodynamic models are widely observed
 235 on Earth for narrow subduction zones. The Gibraltar slab is the clear example of this
 236 geometry (Figure 4a). Our results have demonstrated that including an OP facilitates
 237 the formation of “w”-shaped geometries. For example, our model with $W = 1200$ km
 238 and $\mu_{TF} = 10^{20}$ Pa s develops a “w”-shape (Figure 2c) for much smaller W than any of
 239 the previous studies not using an OP (e.g., F. Chen et al., 2022; Schellart et al., 2007;
 240 Stegman et al., 2010; Strak & Schellart, 2016). Increasing the thickness of the OP has
 241 also been shown to affect the geometry of the trench, with a OP 100 km thick leading to a
 242 “w”-shaped geometry (Figure 3b). This effect of the OP could explain why some natural
 243 subduction zones of narrow to intermediate widths develop “w”-shapes. For example, the
 244 Manila trench ($W = 1000$ km) has a geometry between concave and “w”-shaped (Figure

245 4c) and the Hellenic Arc ($W = 1700$ km) shows a clear “w”-shape (Figure 4b), with a much
246 narrower W than those predicted by previous studies not including an OP.

247 The decrease in V_T with increasing W observed in the present work for $W \geq 800$ km
248 (Figures 2d and 2e) and in previous works (e.g., F. Chen et al., 2022; Royden & Husson,
249 2006; Schellart et al., 2007; Stegman et al., 2006) is in general agreement with observations in
250 narrow and wide subduction zones. This result explains why narrow subduction zones (e.g.
251 Calabria, South Shetland, Halmahera) exhibit relatively high V_T , while wide subduction
252 zones (e.g. Melanesia, South America) are essentially stationary (Schellart et al., 2007).
253 However, when this comparison is restricted to narrow subduction zones, no such correlation
254 is observed (Figure 4d). For the same slab width (~ 900 km), the Makran subduction zone
255 has a V_T of 0.2 cm/yr while the Trobriand system has a V_T of 7.6 cm/yr. Our results showing
256 that W has little effect on V_T for narrow subduction zones, with variations in $V_T \leq 1$ cm/yr
257 (Figure 2e), are in agreement with the lack of correlation between W and V_T observed in
258 nature and provide an explanation for these observations. In contrast, our models reveal
259 that the effect of OP thickness is much stronger, showing an inverse dependence of V_T on
260 OP thickness (Figure 3e). This tendency is also observed in nature for narrow subduction
261 zones (Figure 4e) and brings an explanation of why two subduction zones with the same W
262 (such as Makran and Trobriand) show such different V_T .

263 5 Conclusions

264 The 3-D numerical subduction models presented in this work shed light on some factors
265 (slab width, overriding plate thickness and coupling of the slab with the lateral plate)
266 controlling trench kinematics in narrow subduction zones, and help to explain some obser-
267 vations of natural subduction processes. As opposed to what happens in wide subduction
268 zones, our models show that the slab width has little effect on trench retreat velocities for
269 narrow subduction zones, which is consistent with the lack of correlation between these
270 parameters observed in nature. In contrast, from our models and observations in nature we
271 conclude that the thickness of the overriding plate is the main controlling factor on trench
272 retreat velocities for narrow subduction zones, with velocities decreasing as the thickness in-
273 creases. The strength of slab coupling to the lateral plate is only significant for very narrow
274 subduction zones. Finally, the inclusion of an overriding plate plays an important role in
275 modulating trench geometries, facilitating the formation of “w”-shaped geometries, which
276 are predicted for smaller slab widths than in previous studies.

277 6 Open Research

278 The version 2.4.0 of ASPECT used in this study is available at [https://zenodo.org/](https://zenodo.org/record/6903424)
279 record/6903424. All the information and parameters of the models of this work can be
280 found in the Methods section, in Text S1 and S2 in the supporting information and in
281 Table S1 in the supporting information. The files required to reproduce our simulations are
282 available on https://github.com/Pedrogea08/Gea_et_al_2023GRL.

283 Acknowledgments

284 This work has been funded by Spanish Ministry of Science and Innovation projects PID
285 2019-109608GB-I00, PGC 2018-095154-B-I00 and PID 2020-114854GB-C22 and FEDER-
286 Junta de Andalucía-Conserjería de Economía y Conocimiento/B-RNM-528-UGR20. The
287 computing time was provided by the the Centro de Servicios de Informática y Redes de Co-
288 municacióñ (CSIRC), Universidad de Granada and by the Hamilton HPC cluster, University
289 of Durham. We also thank the Computational Infrastructure for Geodynamics (geodyn-
290 amics.org) which is funded by the National Science Foundation under award EAR-0949446 and
291 EAR-1550901 for supporting the development of ASPECT.

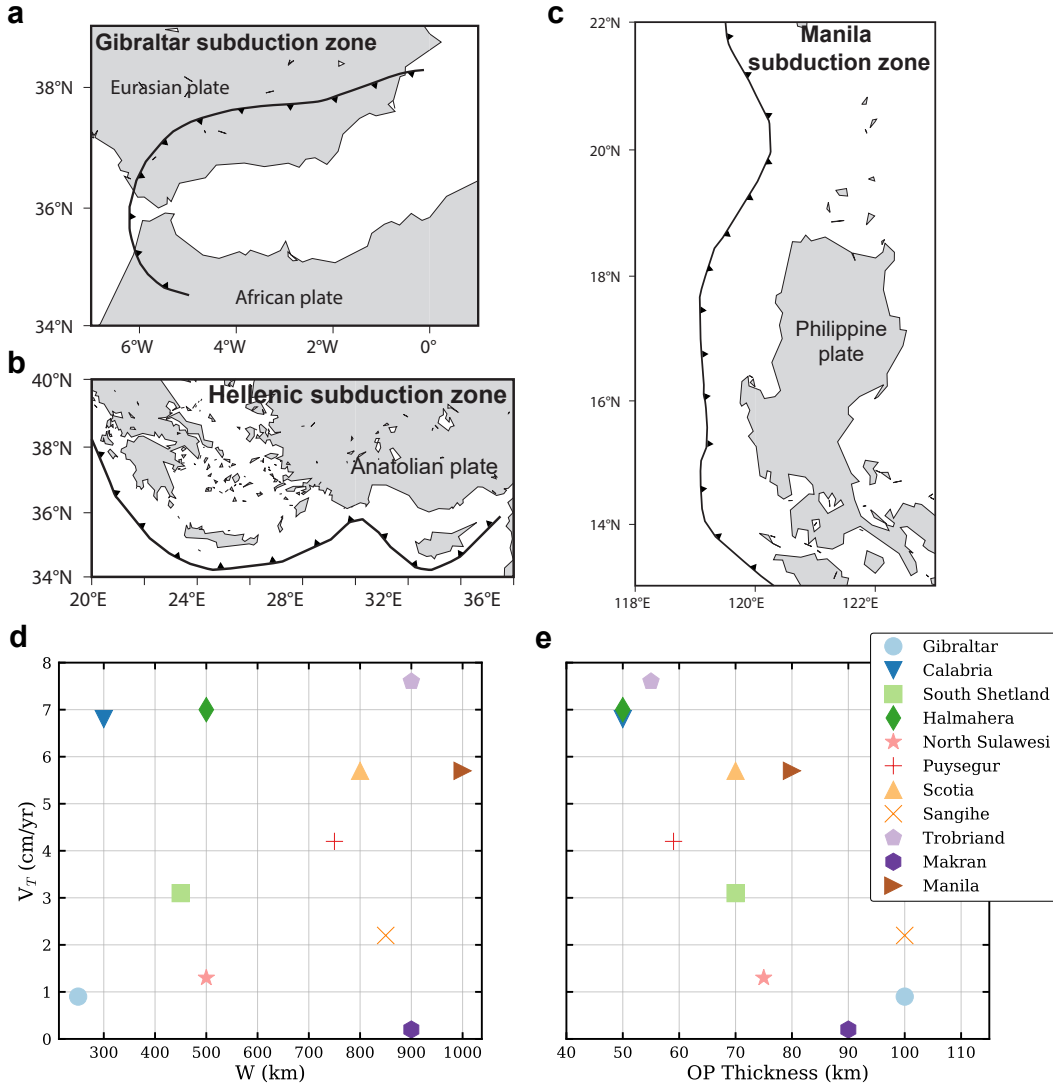


Figure 4. (a-c) Subduction fronts at present-day for the (a) Gibraltar subduction system (from Gutscher et al. (2012)), (b) Hellenic subduction zone (from Lemenkova (2021)) and (c) Manila subduction zone (from Qiu et al. (2019)). (c) V_T against W for all subduction zones in Earth with $W \leq 1000$ km (data from Schellart et al. (2007)). (e) V_T against OP thickness for all subduction zones in Earth with $W \leq 1000$ km (data can be found in table S3 in the supporting information).

293 **References**

- Bangerth, W., Dannberg, J., Fraters, M., Gassmoeller, R., Glerum, A., Heister, T., & Naliboff, J. (2021a, July). ASPECT: *Advanced Solver for Problems in Earth's ConvecTion, User Manual*. doi: 10.6084/m9.figshare.4865333
- Bangerth, W., Dannberg, J., Fraters, M., Gassmoeller, R., Glerum, A., Heister, T., & Naliboff, J. (2021b, July). *Aspect v2.4.0-pre*. Zenodo. doi: 10.5281/zenodo.5131909
- Behr, W. M., Holt, A. F., Becker, T. W., & Faccenna, C. (2022, 02). The effects of plate interface rheology on subduction kinematics and dynamics. *Geophysical Journal International*, 230(2), 796-812. doi: 10.1093/gji/ggac075
- Bellahsen, N., Faccenna, C., & Funiciello, F. (2005). Dynamics of subduction and plate motion in laboratory experiments: Insights into the “plate tectonics” behavior of the earth. *Journal of Geophysical Research: Solid Earth*, 110(B1). doi: 10.1029/2004JB002999
- Billen, M. I. (2008). Modeling the dynamics of subducting slabs. *Annual Review of Earth and Planetary Sciences*, 36(1), 325-356. doi: 10.1146/annurev.earth.36.031207.124129
- Butterworth, N., Quevedo, L., Morra, G., & Müller, D. (2012, 06). Influence of overriding plate geometry and rheology on subduction. *Geochemistry, Geophysics, Geosystems*, 13, Q06W15. doi: 10.1029/2011GC003968
- Capitanio, F., & Morra, G. (2012). The bending mechanics in a dynamic subduction system: Constraints from numerical modelling and global compilation analysis. *Tectonophysics*, 522-523, 224-234. doi: 10.1016/j.tecto.2011.12.003
- Capitanio, F., Stegman, D., Moresi, L., & Sharples, W. (2010, 03). Upper plate controls on deep subduction, trench migrations and deformations at convergent margins. *Tectonophysics*, 483, 80-92. doi: 10.1016/j.tecto.2009.08.020
- Chen, F., Davies, D. R., Goes, S., Suchoy, L., & Kramer, S. C. (2022). How slab age and width combine to dictate the dynamics and evolution of subduction systems: A 3-d spherical study. *Geochemistry, Geophysics, Geosystems*, 23(11), e2022GC010597. doi: 10.1029/2022GC010597
- Chen, Z., Schellart, W., & Duarte, J. (2015, 10). Overriding plate deformation and variability of fore-arc deformation during subduction: Insight from geodynamic models and application to the calabria subduction zone. *Geochemistry Geophysics Geosystems*. doi: 10.1002/2015GC005958
- Di Giuseppe, E., van Hunen, J., Funiciello, F., Faccenna, C., & Giardini, D. (2008). Slab stiffness control of trench motion: Insights from numerical models. *Geochemistry, Geophysics, Geosystems*, 9(2). doi: 10.1029/2007GC001776
- Fraters, M., et al. (2021, July). *The Geodynamic World Builder v0.4.0*. Zenodo. (Zenodo. doi:10.5281/zenodo.5014808) doi: 10.5281/zenodo.5014808
- Fraters, M., Thieulot, C., van den Berg, A., & Spakman, W. (2019). The Geodynamic World Builder: a solution for complex initial conditions in numerical modeling. *Solid Earth*, 10(5), 1785–1807. doi: 10.5194/se-10-1785-2019
- Funiciello, F., Faccenna, C., & Giardini, D. (2004, 06). Role of lateral mantle flow in the evolution of subduction systems: insights from laboratory experiments. *Geophysical Journal International*, 157(3), 1393-1406. doi: 10.1111/j.1365-246X.2004.02313.x
- Funiciello, F., Faccenna, C., Giardini, D., & Regenauer-Lieb, K. (2003). Dynamics of retreating slabs: 2. insights from three-dimensional laboratory experiments. *Journal of Geophysical Research: Solid Earth*, 108(B4). doi: 10.1029/2001JB000896
- Funiciello, F., Faccenna, C., Heuret, A., Lallemand, S., Di Giuseppe, E., & Becker, T. (2008). Trench migration, net rotation and slab–mantle coupling. *Earth and Planetary Science Letters*, 271(1), 233-240. doi: 10.1016/j.epsl.2008.04.006
- Gassmöller, R., Lokavarapu, H., Heien, E., Puckett, E. G., & Bangerth, W. (2018). Flexible and scalable particle-in-cell methods with adaptive mesh refinement for geodynamic computations. *Geochemistry, Geophysics, Geosystems*, 19(9), 3596–3604. doi: 10.1029/2018GC007508
- Gea, P. J., Negredo, A. M., & Mancilla, F. d. L. (2023). The gibraltar slab dynamics and its influence on past and present-day alboran domain deformation: Insights from

- 348 thermo-mechanical numerical modelling. *Frontiers in Earth Science*, 11. doi: 10.3389/
 349 feart.2023.995041
- 350 Gerya, T. (2022, 02). Numerical modeling of subduction: State of the art and future
 351 directions. *Geosphere*, 18(2), 503-561. doi: 10.1130/GES02416.1
- 352 Guillaume, B., Funiciello, F., & Faccenna, C. (2021). Interplays between mantle flow and
 353 slab pull at subduction zones in 3d. *Journal of Geophysical Research: Solid Earth*,
 354 126(5), e2020JB021574. doi: 10.1029/2020JB021574
- 355 Guillaume, B., Funiciello, F., Faccenna, C., Martinod, J., & Olivetti, V. (2010, 09). Spreading
 356 pulses of the Tyrrhenian Sea during the narrowing of the Calabrian slab. *Geology*,
 357 38(9), 819-822. doi: 10.1130/G31038.1
- 358 Gutscher, M.-A., Dominguez, S., Westbrook, G., Le Roy, P., Rosas, F., Duarte, J., ...
 359 Bartolome, R. (2012). The gibraltar subduction: A decade of new geophysical data.
 360 *Tectonophysics*, 574-575, 72-91. doi: 10.1016/j.tecto.2012.08.038
- 361 Heister, T., Dannberg, J., Gassmöller, R., & Bangerth, W. (2017). High accuracy mantle
 362 convection simulation through modern numerical methods. II: Realistic models and
 363 problems. *Geophysical Journal International*, 210(2), 833-851. doi: 10.1093/gji/
 364 ggx195
- 365 Hertgen, S., Yamato, P., Guillaume, B., Magni, V., Schliffke, N., & van Hunen, J. (2020,
 366 01). Influence of the thickness of the overriding plate on convergence zone dynam-
 367 ics. *Geochemistry, Geophysics, Geosystems*, 21, e2019GC008678. doi: 10.1029/
 368 2019GC008678
- 369 Holt, A., Becker, T., & Buffett, B. (2015, 02). Trench migration and overriding plate stress
 370 in dynamic subduction models. *Geophysical Journal International*, 201, 172-192. doi:
 371 10.1093/gji/ggv011
- 372 Holt, A. F., & Becker, T. W. (2016, 10). The effect of a power-law mantle viscosity on
 373 trench retreat rate. *Geophysical Journal International*, 208(1), 491-507. doi: 10.1093/
 374 gjj/ggw392
- 375 Kronbichler, M., Heister, T., & Bangerth, W. (2012). High accuracy mantle convection
 376 simulation through modern numerical methods. *Geophysical Journal International*,
 377 191, 12-29. doi: 10.1111/j.1365-246X.2012.05609.x
- 378 Lemenkova, P. (2021, 09). Submarine tectonic geomorphology of the pliny and hellenic
 379 trenches reflecting the geological evolution of southern greece. *Rudarsko Geolosko
 380 Naftni Zbornik*, 36, 33-48. doi: 10.17794/rgn.2021.4.4
- 381 Magni, V., Faccenna, C., van Hunen, J., & Funiciello, F. (2014, 06). How collision triggers
 382 backarc extension: Insight into Mediterranean style of extension from 3-D numerical
 383 models. *Geology*, 42(6), 511-514. doi: 10.1130/G35446.1
- 384 Meyer, C., & Schellart, W. P. (2013). Three-dimensional dynamic models of subduct-
 385 ing plate-overriding plate-upper mantle interaction. *Journal of Geophysical Research:
 386 Solid Earth*, 118(2), 775-790. doi: 10.1002/jgrb.50078
- 387 Piromallo, C., Becker, T. W., Funiciello, F., & Faccenna, C. (2006). Three-dimensional in-
 388 tantaneous mantle flow induced by subduction. *Geophysical Research Letters*, 33(8).
 389 doi: 10.1029/2005GL025390
- 390 Pusok, A., Kaus, B., & Popov, A. (2018, 05). The effect of rheological approximations in
 391 3-d numerical simulations of subduction and collision. *Tectonophysics*, 746, 296-311.
 392 doi: 10.1016/j.tecto.2018.04.017
- 393 Qiu, Q., Li, L., Hsu, Y.-J., Wang, Y., Chan, C.-H., & Switzer, A. D. (2019). Revised
 394 earthquake sources along manila trench for tsunami hazard assessment in the south
 395 china sea. *Natural Hazards and Earth System Sciences*, 19(7), 1565–1583. doi: 10
 396 .5194/nhess-19-1565-2019
- 397 Rodríguez-González, J., Billen, M. I., & Negredo, A. M. (2014). Non-steady-state subduction
 398 and trench-parallel flow induced by overriding plate structure. *Earth and Planetary
 399 Science Letters*, 401, 227-235. doi: 10.1016/j.epsl.2014.06.013
- 400 Royden, L. H., & Husson, L. (2006, 11). Trench motion, slab geometry and viscous stresses
 401 in subduction systems. *Geophysical Journal International*, 167(2), 881-905. doi:
 402 10.1111/j.1365-246X.2006.03079.x

- 403 Schellart, W. P. (2004). Kinematics of subduction and subduction-induced flow in the
404 upper mantle. *Journal of Geophysical Research: Solid Earth*, 109(B7). doi: 10.1029/
405 2004JB002970
- 406 Schellart, W. P. (2008). Kinematics and flow patterns in deep mantle and upper mantle
407 subduction models: Influence of the mantle depth and slab to mantle viscosity ratio.
408 *Geochemistry, Geophysics, Geosystems*, 9(3). doi: 10.1029/2007GC001656
- 409 Schellart, W. P., Freeman, J., Stegman, D., Moresi, L., & May, D. (2007, 03). Evolution
410 and diversity of subduction zones controlled by slab width. *Nature*, 446, 308-11. doi:
411 10.1038/nature05615
- 412 Sharples, W., Jadamec, M. A., Moresi, L. N., & Capitanio, F. A. (2014). Overriding
413 plate controls on subduction evolution. *Journal of Geophysical Research: Solid Earth*,
414 119(8), 6684-6704. doi: 10.1002/2014JB011163
- 415 Stegman, D., Farrington, R., Capitanio, F., & Schellart, W. (2010). A regime diagram
416 for subduction styles from 3-d numerical models of free subduction. *Tectonophysics*,
417 483(1), 29-45. (Convergent plate margin dynamics: New perspectives from structural
418 geology, geophysics and geodynamic modelling) doi: 10.1016/j.tecto.2009.08.041
- 419 Stegman, D., Freeman, J., Schellart, W., Moresi, L., & May, D. (2006, 03). Influence
420 of trench width on subduction hinge retreat rates in 3-d models of slab rollback.
421 *Geochemistry Geophysics Geosystems*, 3060. doi: 10.1029/2005GC001056
- 422 Strak, V., & Schellart, W. P. (2016). Control of slab width on subduction-induced up-
423 per mantle flow and associated upwellings: Insights from analog models. *Journal of
424 Geophysical Research: Solid Earth*, 121(6), 4641-4654. doi: 10.1002/2015JB012545
- 425 van Hunen, J., & Allen, M. B. (2011). Continental collision and slab break-off: A comparison
426 of 3-d numerical models with observations. *Earth and Planetary Science Letters*,
427 302(1), 27-37. doi: 10.1016/j.epsl.2010.11.035
- 428 Xue, K., Schellart, W. P., & Strak, V. (2020). Effect of plate length on subduction kine-
429 matics and slab geometry: Insights from buoyancy-driven analog subduction mod-
430 els. *Journal of Geophysical Research: Solid Earth*, 125(11), e2020JB020514. doi:
431 10.1029/2020JB020514
- 432 Yamato, P., Husson, L., Braun, J., Loiselet, C., & Thieulot, C. (2009, 04). Influence
433 of surrounding plates on 3d subduction dynamics. *Geophysical Research Letters -
434 GEOPHYS RES LETT*, 36, L07303. doi: 10.1029/2008GL036942
- 435 Čížková, H., & Bina, C. R. (2013). Effects of mantle and subduction-interface rheologies
436 on slab stagnation and trench rollback. *Earth and Planetary Science Letters*, 379,
437 95-103. doi: 10.1016/j.epsl.2013.08.011
- 438 Čížková, H., & Bina, C. R. (2019). Linked influences on slab stagnation: Interplay between
439 lower mantle viscosity structure, phase transitions, and plate coupling. *Earth and
440 Planetary Science Letters*, 509, 88-99. doi: 10.1016/j.epsl.2018.12.027

Figure 1.

$T_s = 293 \text{ K}$

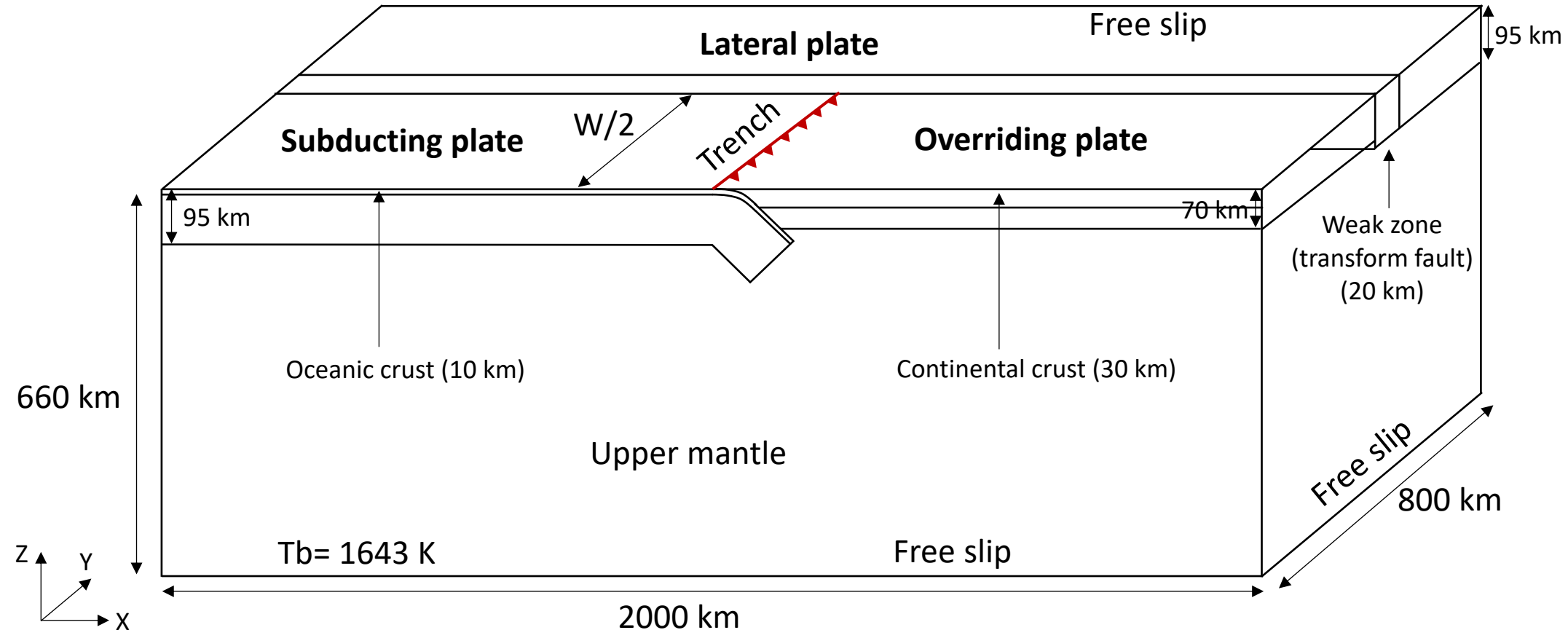


Figure 2.

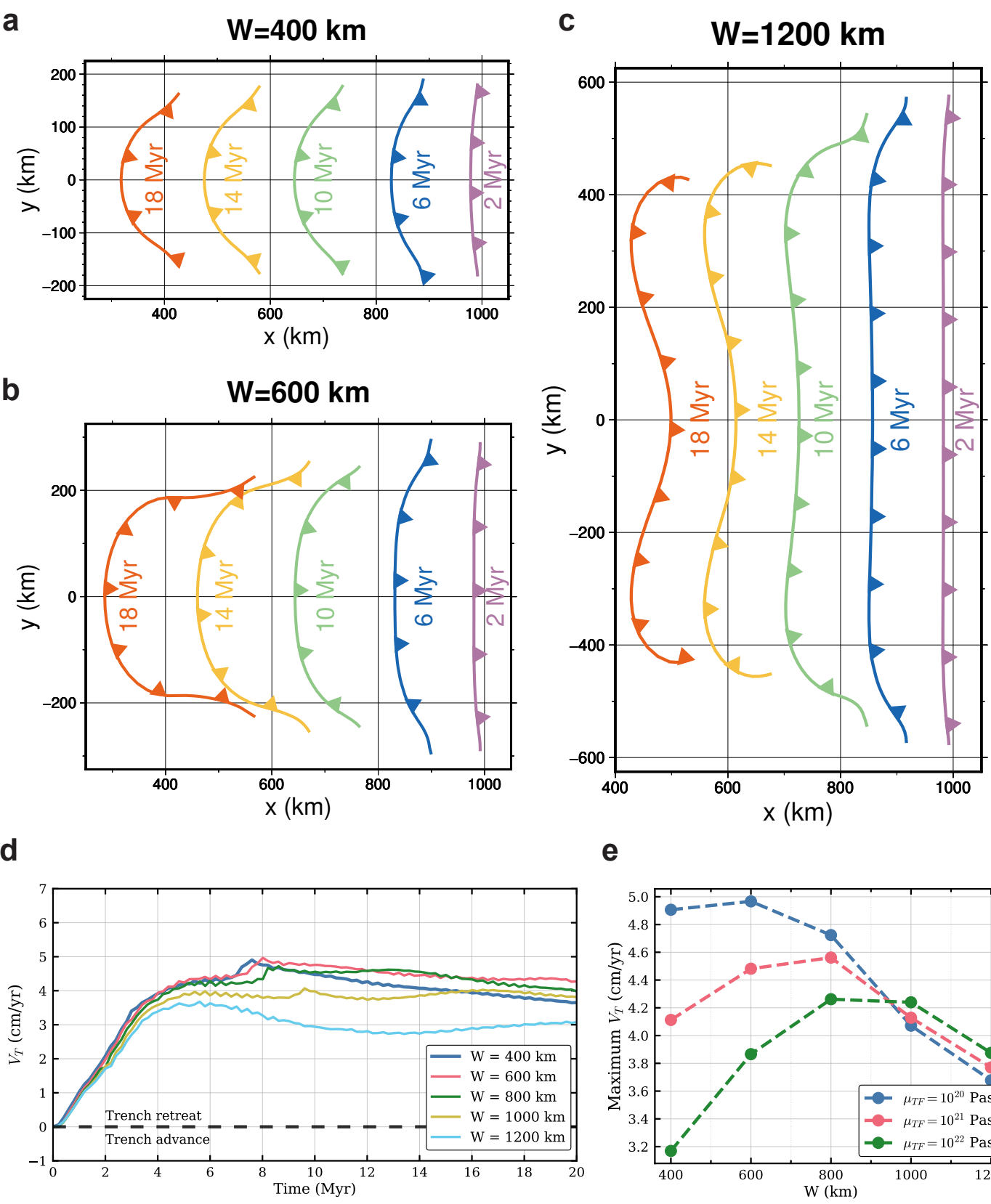


Figure 3.

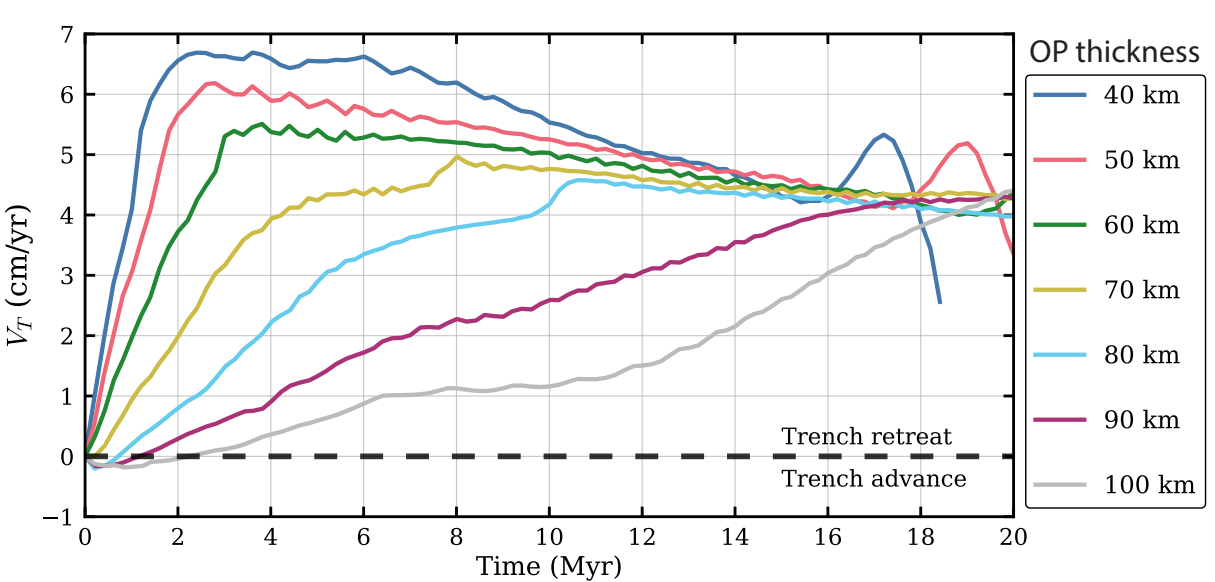
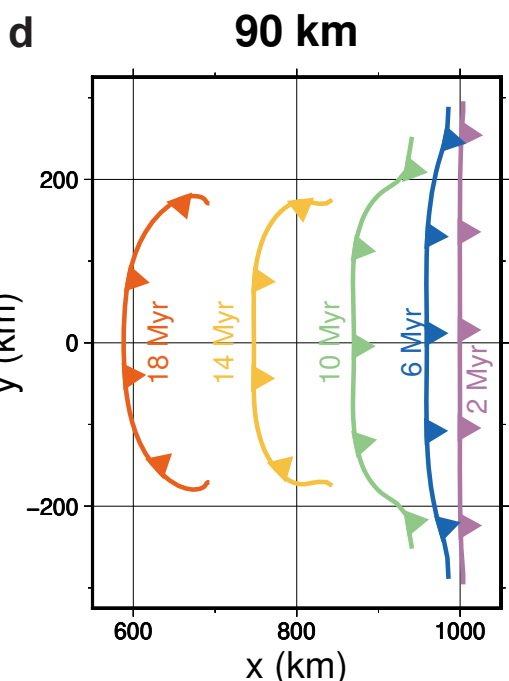
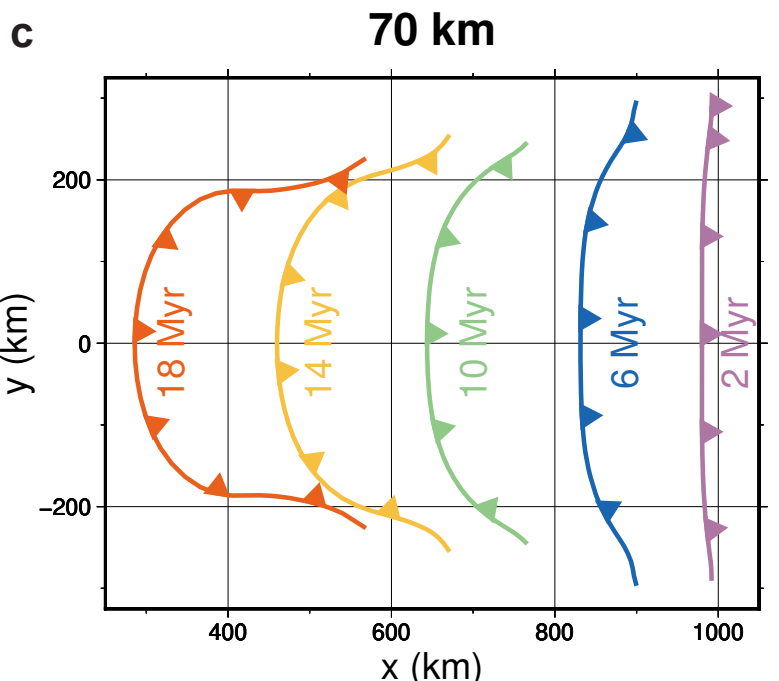
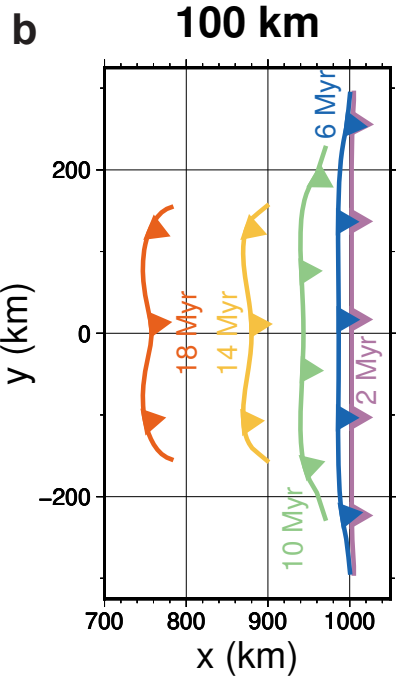
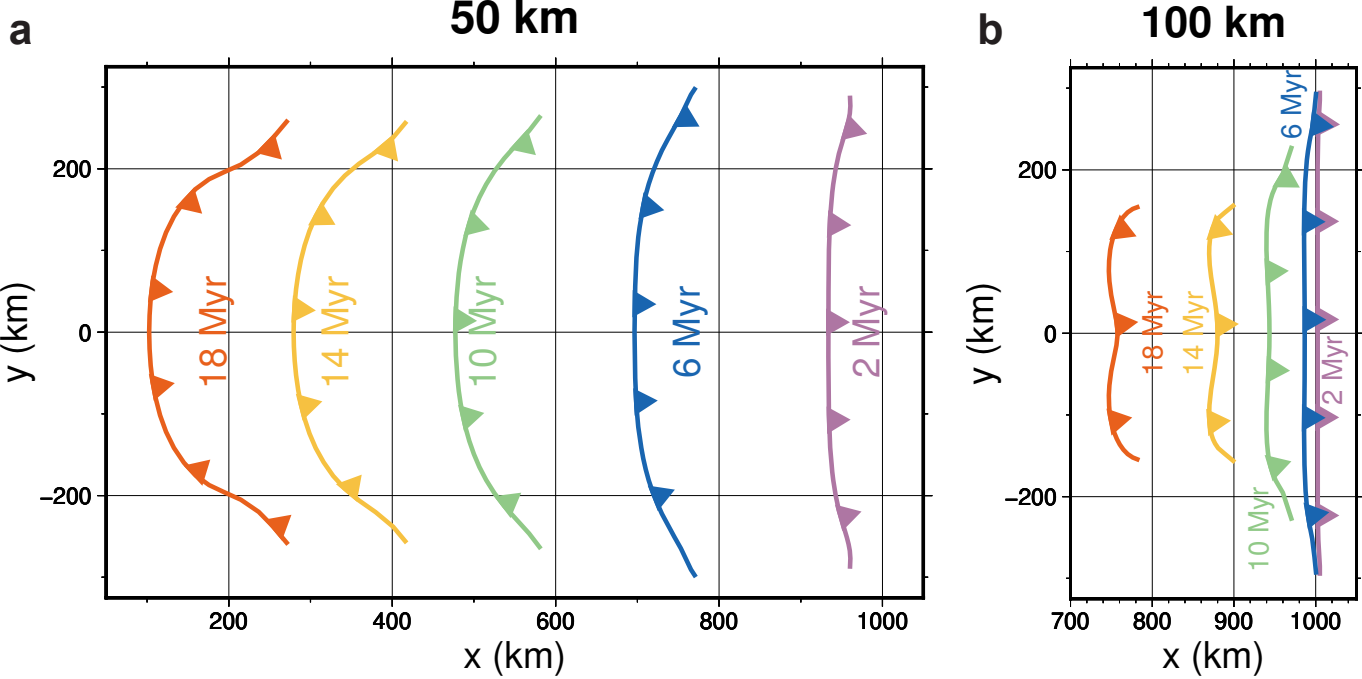


Figure 4.

